

Extreme outflow of Enormous Ly α Nebula in MAMMOTH-1

Shiwu Zhang¹ and Zheng Cai¹

¹Department of Astronomy, Tsinghua University, Shuangqing Road No.30, Haidian Beijing China

Abstract

1. Introduction

In the local universe, most galaxies are found massive cluster with a giant elliptical galaxy locating at center. The current hierarchical structure formation model predicts that these central galaxies merge with several nearby satellite galaxies to build up their stellar mass. This violent merging process is thought to take place in the highest density peaks in the early Universe, the so-called protoclusters. There are several decades year efforts on searching for these structures at high-redshift and some methods have been proposed. However it is still under debates that on which systems represent the nurseries of present-day massive clusters.

Previous work searching for protocluster base on high-redshift radio galaxies(HzRGs). This method is supported by Lyman α emitters(LAEs) overdensities near them, and in some cases by overdensities in submillimeter observations. Being the host of active galactic nucleus(AGN) and characterized by intense radio emission, HzRGs are also known for their associated giant Lyman α nebulae on hundreds of kpc scales. However, ? proposed a new method(MAMMOTH: mapping the most massive overdensity through hydrogen) to search for overdensities. With this approach ? discovered an extremely massive overdensity BOSS1441 at $z=2.32$. Through narrow band observation with Large Binocular Telescope(LBT),? found an enormous lyman α nebulae(ELANe) projected distance of which is beyond 400kpc. This is also the largest ELANes ever discovered. In the cosmic hierarchical nature of structure formation, large-scale filaments are formed out of the merging of small-scale pieces. Simulations suggest that cosmic webs containing baryonic matter tend to align with underlying large-scale structures of dark matter. So, the discovery of such large scale nebulae is a strong evidence of cosmic large-scale structure and the hierarchical model of galaxies formation.

Futhermore, the long-slit observations indicate the ELANe of MAMMOTH-1 has a drastically different kinematics compared to previously discovered ELANes. It is the first radio-quiet nebulae that is associated with strongly extended HeII CIV OIII and H α emission. The emission lines can be fit by two major components about 1000km/s. These results suggests there is strong feedback powered by central AGN. AGN are fascinating objects, the huge amounts of energy released by the active super massive black hole(SMBH) can

have an impact on the life and evolution of their entire host galaxy. This process is called AGN feedback, which is a key ingredient in the theory model of galaxies evolution. AGN feedback is now included in many theoretical, numerical and semi-analytic models. The goal of the observations is to provide constraints to help a realistic implementation of feedback effects in simulations. several evidences show powerful outflow from AGN. sturm 2011 used Herschel-PACS find high velocities above 1000 km/s and mass outflow rate $M \approx 1200M_{\odot}/yr$ in Ultra-Luminous Infared Galaxies(ULIRGs). There're also many reports of outflows from galaxies hosting AGN 1000 km/s outflows have been seen either side of an obscured quasar at low redshifts. Besides, there are also strong outflows observed at high redshifts. In most cases outflows are discovered by metal absorption lines such as OIII or CII. This is a direct method because there's more material in galaxies and we can estimate its peculiar velocity by spectra. A spectacular examples is the 1300 km/s outflow in a quasar at $z \approx 6.4$ revealed by broad wings of CII emission line. The kinetic power in the outflow is $\dot{E} \approx 2 \times 10^{45} erg/s$.

In this paper we present Keck Cosmic Web Imager(KCWI) blue sensitive Integral Field Spectrometer(IFS) observation of MAMMOTH-1 which is the denest region ever seen at $z \approx 2$. In section 2 we give details of IFU observations, In section 3 we present the results and model used to estimate outflow energy. Finally we discuss the Lyman α nebula and the possible mechanism to power the strong outflow, and give a brief summary in section 5. Throughout this paper, we assume a flat cosmological model with $\omega_{\Lambda} = 0.7, \omega_m = 0.3$ and $H_0 = 70 km/s/Mpc$. In this cosmology, $1'' \approx 8 kpc$.

2. Observations

In this section, we provide details on the KCWI instrument configurations, observations,data reduction pipeline, and post-processing after standard reduction pipeline

2.1. KCWI Instrument Configuration

Keck Cosmic Web Imager(KCWI) is a general purpose, optical IFS that has been installed on the 10m Keck II telescope. KCWI provides seeing-limited imaging from the wavelength of 3500 – 5700, and the spectral resolution can be configured from R=1000 to R=20000. The field of view is $20'' \times 33''$ for large slicer, $16'' \times 20''$ for medium slicer and $8'' \times 20''$ for the small slicer. KCWI is optimal for a survey of gasous nebulae at $z \approx 2$ because: (1) KCWI has a high throughput from 3800 – 4500, optimal for probing Lyman α

CIV and HeII lines at $z \approx 2$. (2) KCWI has a high spectral-resolution modes($R > 4000$) which resolve the gas kinematics and (3) KCWI has a relatively large field-of-view(FoV) to cover extended Lyman α nebulae. Furthermore, KCWI nicely complements the characteristics of MUSE which thrives at $\lambda > 5000$. Data was taken with the Keck/KCWI instrument in November 2017. The seeing varied in the range of 0.7-1.1 arcsec.

3. Results

3.1. Radio Emission

Deep VLA observation on MAMMOTH-1 with 2.3" resolution (see ?) shows radio CO(1-0) emission which can trace the cold molecular gas (T 10-100 K) on source-B and its companions. He used D-configuration of VLA and centered on the frequency of 34.808 GHz($\nu_{rest} = 115.27$ GHz). After 14 hrs exposure, the results shows extended peak radio flux which has 5 kpc offset from the stellar body of source-B (30 kpc beyond 3σ). Besides, he also detected 3 faint radio sources in the same region. With CO(1-0) emission he calculated the total mass of molecular gas $M_{H_2} = 1.4(\alpha_{CO}/3, 6) \times 10^{11} M_\odot$, furthermore, he found an unusually narrow velocity dispersion(FWHM 85 km/s), follows diffuse light seen in HST imaging, he interprets that this molecular CGM in the core likely originated from gas cooling in an enriched multi-phase medium.

From the results of ?, we doesn't get any confident detection of continuum radio source at the position of Source-B. However, we give an upper limit on its submillimeter emission, $f_\nu < 0.01 mJy$ at $\lambda_{obs} = 8500\mu m$. But from the results of ?(Figure 11), this upper limit still cannot rule out the the radio-loud case. But neither the VLA nor ALMA observations detected two distinct radio sources around Source-B, we conclude that Source-B is most likely radio-quiet source.

3.2. Morphology and Emission

Fig. ?? shows the HST image of MAMMOTH-1 with WFC F160W filter and contours for Ly α HeII and CIV emission. All sources marked here are at $z=2.3$ (confirmed by CO(1-0) emission from Emonts et al. (2019) and Qiong (prep)). It shows Ly α emission extended $> 20''$ which corresponds to ≈ 170 kpc at this redshift, this is the typical size of halo at this redshift. It covers all 8 sources here, this indicates that all of this sources could have contribution to illuminate this nebulae. We don't see this nebulae all because FoV of KCWI is $20'' \times 16.8''$ and it's not that sensitive at the edges. Besides Ly α . Also we see HeII and CIV emission, contour shows signal beyond 3σ and 4σ for these 2 lines respectively. These 2 emissions are also extent because their size $>$ seeing and velocity gradient weighted from these 2 lines is significant (we would not see it if they are not resolved). The contour shows these 2 emission extended $> 6''$ which corresponds to physical projected scale of 50 kpc. Besides, We don't find any significant HeII or CIV emission around other sources.

Fig. ?? shows spectra extract in 1 arcsec^2 aperture centering on the flux peaks. We fit the 3 emission lines with one-component gaussian function and also use the central wavelength fitted to calculate their redshifts, moreover we calculate their luminosity beyond 3σ . We show these results and the fitting parameters in Tab. 1.

	$\lambda_c(A)$	$\sigma_\lambda(A)$	L(erg/s)	redshift
Ly α	4024	7	2.68×10^{44}	2.310
HeII	5438	8	1.97×10^{43}	2.316
CIV	5143	13	2.29×10^{43}	2.320

Table 1: aa

3.3. Kinematics

In this section we present the maps for the flux-weighted velocity centroid and the flux-weighted velocity dispersion of all of the extended emission line to get an indication of the centroid velocity and width of the emission line for each spatial location. Different emission line trace different gas component. We use lyman α to trace cool gas(10^4 K) and use CIV($\lambda 1549$),HeII($\lambda 1640$) emission to trace warm gas(10^5 K). These resolved kinematic maps give us the opportunity to detect kinematic patterns, e.g. evidence for rotation, inflows or outflows and help us to have a deep insight look to the physics of this nebula. We filter the spectra with lowpass filter to reduce the noise, this procedure can help us to construct a more clear velocity and velocity dispersion map, we show the results in Fig. ??

Fig. ?? shows the results. Left panel is the continuum-subtracted, pseudo-narrowband image, contour reperesents the SNR levels. Middle panel shows velocity maps and right panel is velocity dispersion map. Ly α shows 2 peaks, one is around source-B the other is around G-5, moreover we we also see significant velocity gradient close to these 2 peaks in ly α velocity map. Besides, dispersion map also reveals relatively large σ_v around these 2 sources. The 2 clues indicate source-B and G-5 both have outflows. To have a deep insight, we bin the data cube with interval length of 200km/s and show the results in Fig. ?. It shows significant separate red and blue component on either side of source-B. As for G-5, the red component is significant but the blue component is relatively weak.

To further explore the physical mechanism here, we extract spectra from different regions of lyman α nebula and construct a "spectral map", Fig.?? shows the result. We construct aperture with radius of 1 arcsec^2 and extract spectra from different part of Ly α neubulæ. We also fit lines with one-component gaussian function and show the fitting parameter in Tab. ?. We clearly see in some regions close to source-B the dispersion is really large even > 600 km/s which corresponds to FWHM > 1400 km/s. It's hard to imagine anything other than an outflow could cause such a large dispersion.

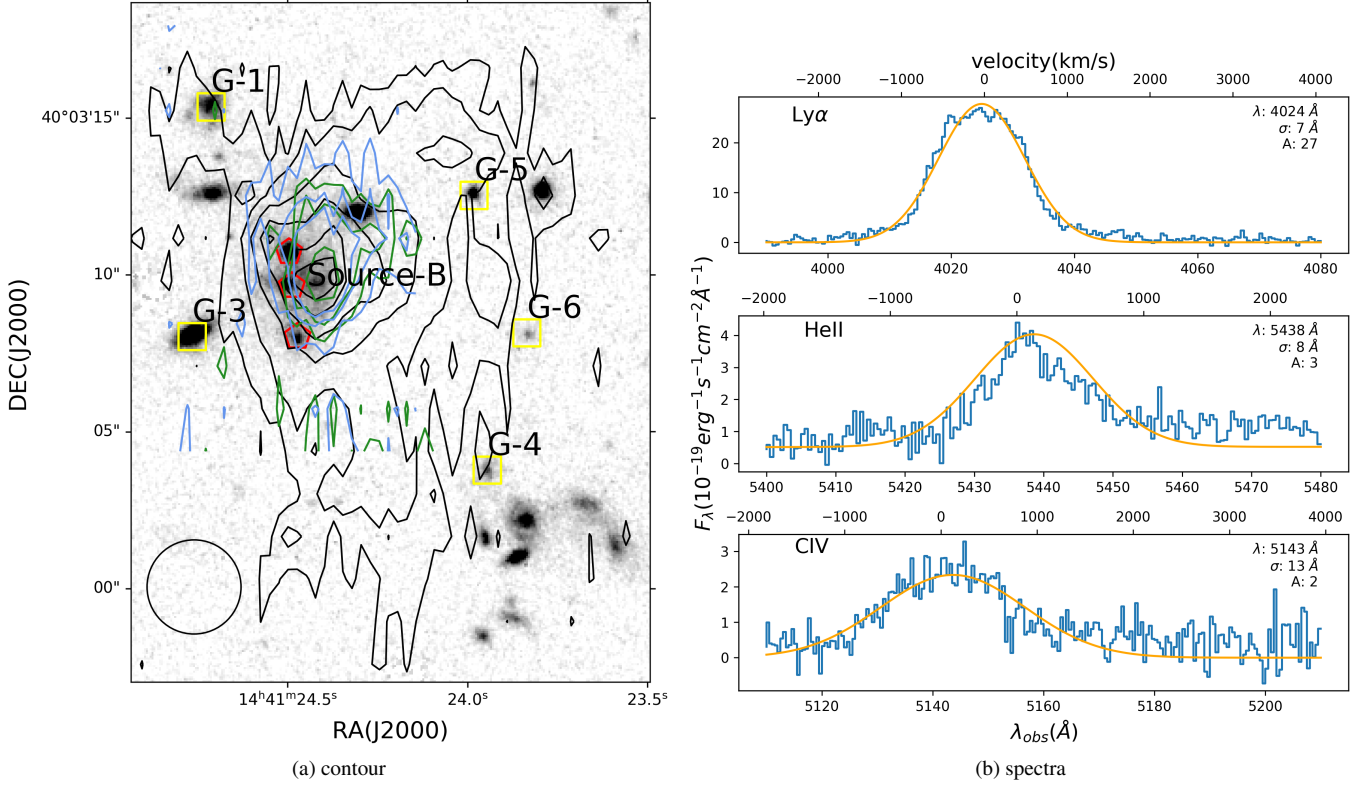


Figure 1: Left: HST image of MAMMOTH-1 from circle 24,25, PI: Cai. We overlay on it Ly α , HeII and CIV pseudo narrow band images. Black contour is Ly α , blue contour is HeII, green contour is CIV. We also mark source-B with red mark and sources at the same redshift with yellow mark. We also plot circle with radius of 1 arcsec 2 . Right: spectra of the 3 emission lines extracted from aperture center on source-B with radius 1 arcsec 2 , we fit them with one-component gaussian function.

3.4. Model of the outflow

The mass rate, energy rate and momentum rate being carried by outflow are important to help us understand the physical mechanisms to drive it. Although outflow are likely to be entraining gas in multiphases, the cool and warm gas observed here could represent a large fraction of the overall mass and energy of the total outflows. Because of the complication of modeling outflows, here we adopt simple outflow models to provide first order constraints. We calculate the upper and lower limit of the outflow energy rate with 2 different ways and the fiducial value we use is their mean in log space (follow the method given by Harrison et al. (2014)). The upper limit is given by Rodriguez Zauri et al. (2013), we use eq. 7 in his paper to calculate the mass outflow rate:

$$\dot{M} = \frac{3Lm_p v_{out}}{\alpha_{Ly\alpha}^{eff} h\nu_{Ly\alpha} n_e r} \quad (1)$$

where L is the luminosity of Lyman α emission, m_p is the proton mass, v_{out} is outflow velocity, $\alpha_{Ly\alpha}^{eff}$ is recombination coefficients, we get this value from Storey & Hummer (1995), $h\nu_{Ly\alpha}$ is the energy of Lyman α photons, n_e is electron density, r is the distance we see the outflow from the central AGN, in our case we adopt 30kpc. In addition, the kinetic

power of the outflow (\dot{E}) is related to the velocity dispersion, mass outflow rate and outflow velocity by:

$$\dot{E} = \frac{\dot{M}}{2} (V_{out}^2 + 3\sigma^2) \quad (2)$$

the main uncertainty in calculating the mass outflow rates is electron density, this value is often measured from the emission-line ratio SII $\lambda 6716/\lambda 6731$, this doublet is not covered by our IFU observations, hence, we adopt the value in Cai et al. (2017) $n_e = 1.25 \text{ cm}^{-3}$. With this approach, we obtain $\dot{M}_{out,low} \approx 500 \text{ M}_\odot \text{ yr}^{-1}$. Moreover with the velocity dispersion we estimated, the energy outflow rate is $\dot{E}_{out,low} \approx 10^{44} \text{ erg/s}$.

We also consider the mass energy injection rates assuming an energy conserving bubble in a uniform medium Heckman et al. (1990) which gives the relation:

$$\dot{E}_{out,up} \approx 1.5 \times 10^{46} r_{10}^2 v_{1000}^3 n_{0.5} \text{ erg/s} \quad (3)$$

where r_{10} is the radius in unit of 10kpc, v_{1000} in unit of 1000km/s and $n_{0.5}$ is in unit of 0.5 cm^{-3} . Using this method we obtain values of $E_{out,up} \approx 9 \times 10^{46} \text{ erg/s}$. The mass outflow rates are then given by $\dot{M}_{out,up} = 2\dot{E}_{out,up}/c^2$ where c is the speed of light, this gives $M_{out,up} \approx 8.7 \times 10^5 \text{ M}_\odot/\text{yr}$. So the fiducial value we use is $\dot{E}_{out,mean} = 3 \times 10^{45} \text{ erg/s}$.

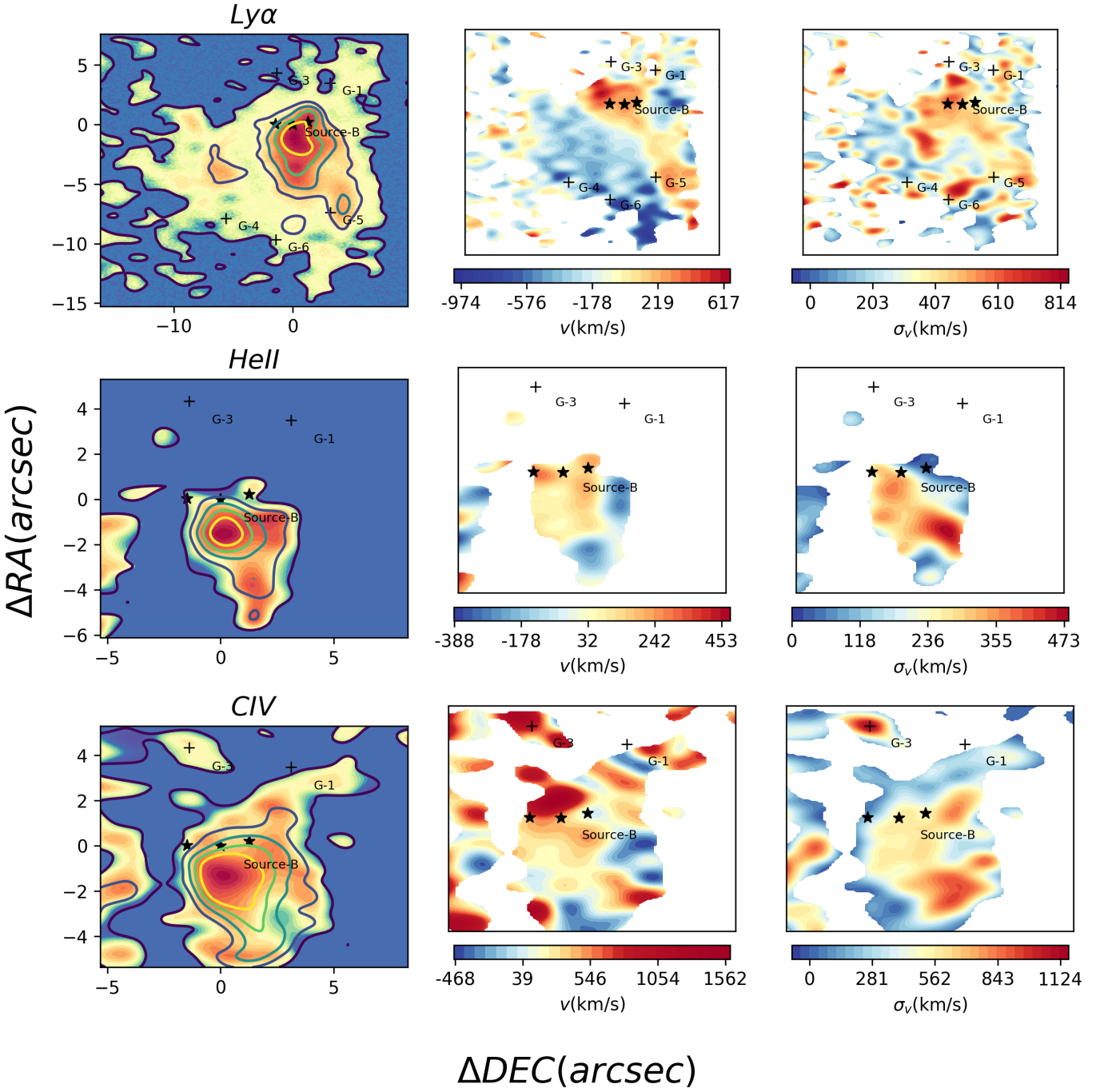


Figure 2: Left: continuum-subtracted pseudo-narrow band images for the 3 emissions. We select regions $> 1.5\sigma$ in each slice and stack these slices together. The contour represent signal-to-noise ratio(SNR), for Ly α is $(5\sigma, 9\sigma, 18\sigma, 30\sigma, 42\sigma, 51\sigma)$, for HeII is $(3\sigma, 5, 9\sigma)$ and for CIV is $(4\sigma, 7\sigma, 9\sigma)$. Middle: flux-weighted velocity map with respect to the systemic redshift of MAMMOTH-1. Right: flux-weighted velocity dispersion also with respect to systemic redshift of MAMMOTH-1. We also mark sources in the field with cross.

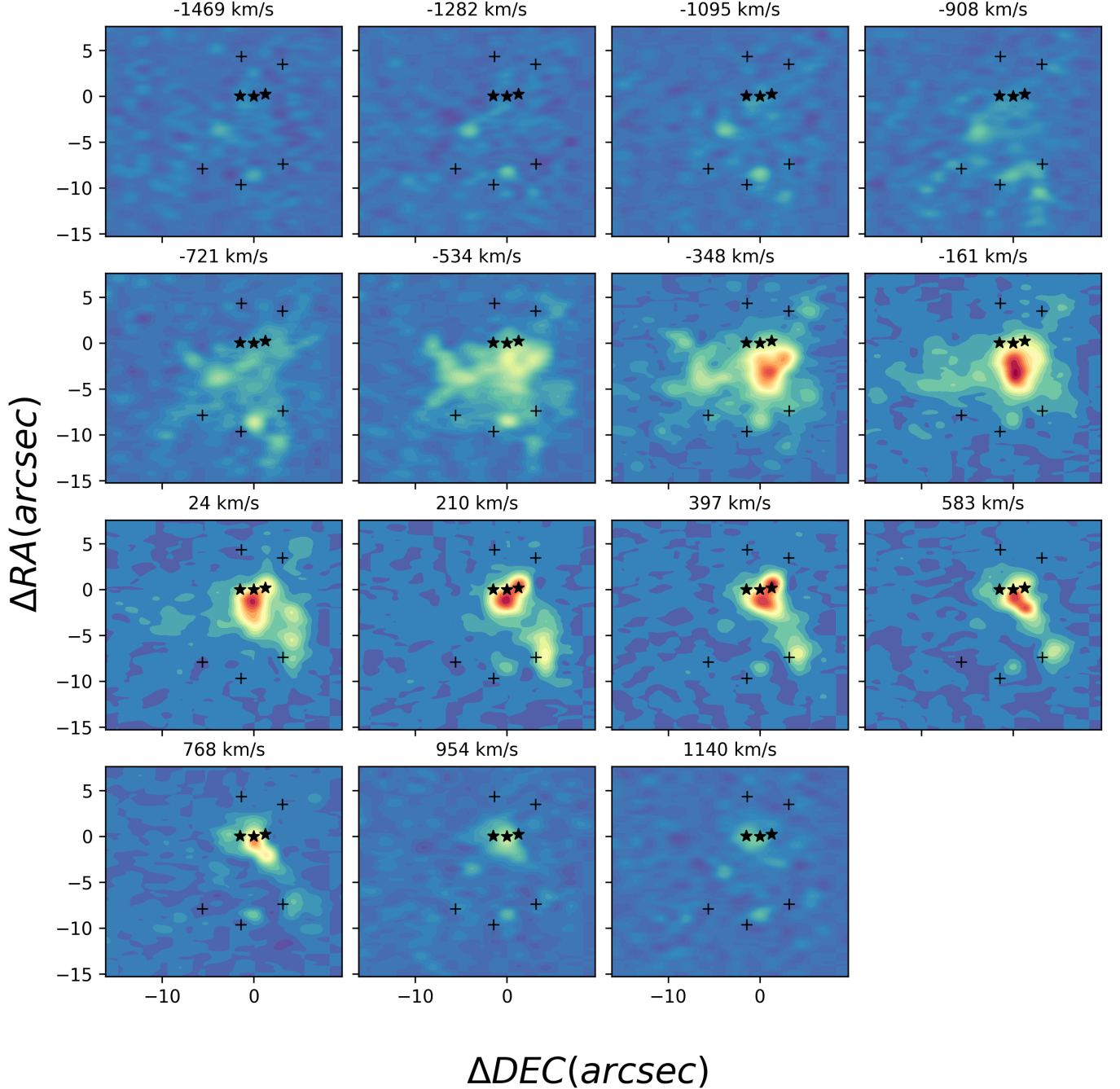


Figure 3: Kinematics of cool gas. It shows signal of Ly α emission at different velocities. We select $\Delta v = 187\text{km/s}$ which corresponds $4A$ as the bin size of these slices. We extract these slices within the range $4000A - 4040A$, for each image here, we use the mean velocity of the bin as title for each image. It shows significant red and blue component on either side of source-B.

Number	1	4	5	7	8	9	10	11	12	13	14	15	16	17	18	19	20	24	25
Velocity(km/s)	-416	-785	-649	-419	-515	-453	208	-157	-257	-424	-211	9	-75	-300	49	236	-267	182	-208
Dispersion(km/s)	618	342	392	626	319	474	450	174	219	444	269	415	799	242	668	481	358	660	472
f_{norm}	0.69	0.63	0.73	0.70	0.79	0.83	0.71	0.84	0.95	0.85	0.91	0.83	0.41	0.86	0.66	0.93	0.81	0.66	0.77

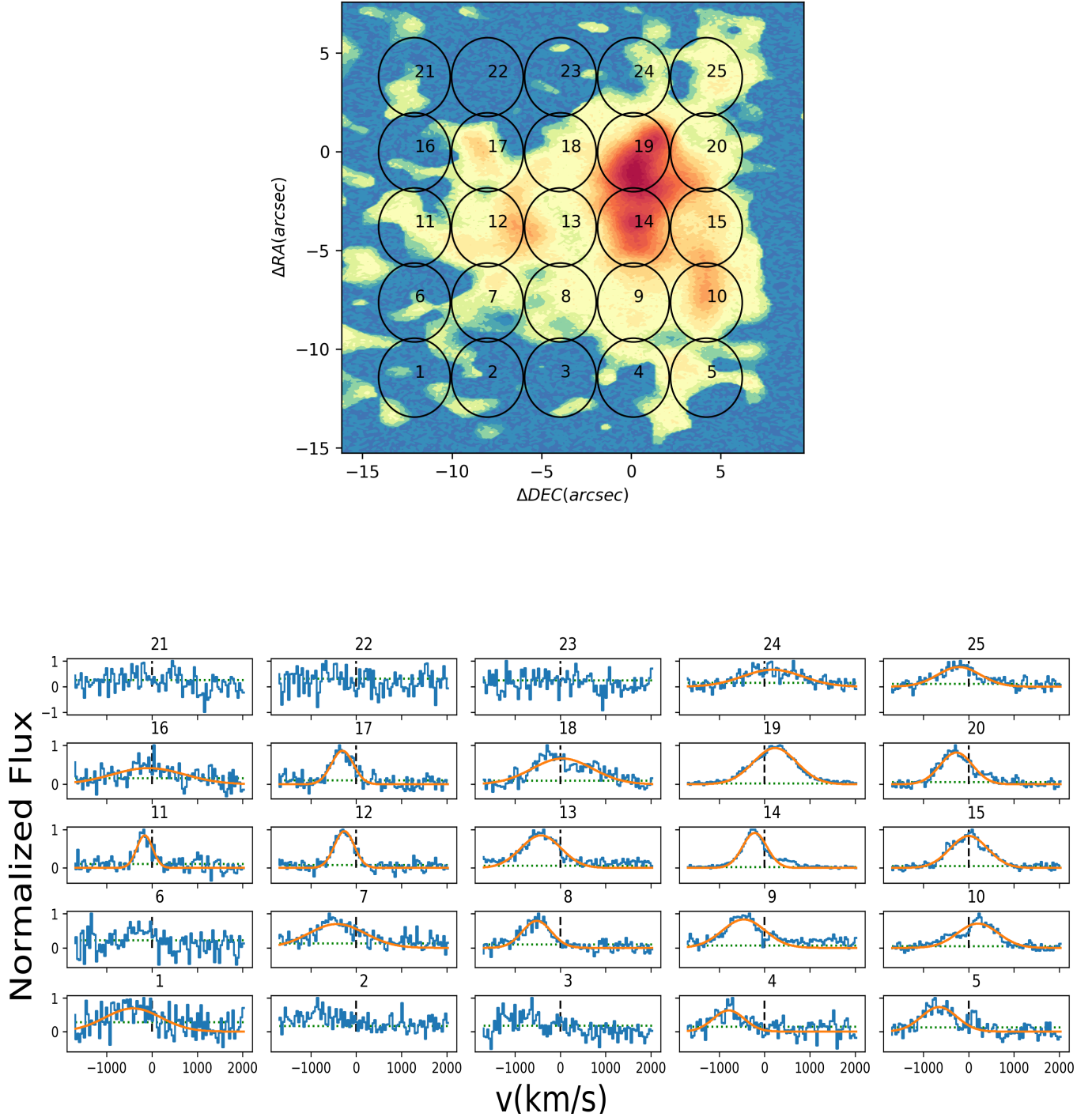


Figure 4: Up: Continuum-subtracted psudo narrow band image of Ly α . We overlay circles on it and number them from 1 to 25. Low: Continuum-subtracted spectra extracted from individual spatial regions indicated in upper panel. The apertures are circle with radius of 2arcsec^2 . We number the spectra from 1 to 25 which corresponds to circles in upper panel. We fit the emission line with single gaussian function and show it with orange lines. The green lines show the noise level calculated from the high-frequency component of spectra.

Finally, in preparation for the follow discussion, we estimate outflow momentum rate by taking the mass outflow rate calculated above and assuming $\dot{P}_{out} = \dot{M}_{out}v_{out}$

4. Discussion

4.1. What drives the outflow?

The dominant processes that drive such large scale outflow in protocluster and the efficiency to which they are able to couple the gas are currently sources of uncertainty in galaxy formation models. Several possible mechanisms have been suggested to drive galaxy-wide outflows, for example: the stellar wind and supernovae; radiation pressure from the extremely luminous AGN or star formation; the interaction of radio jets with a clumpy and multiphase interstellar medium; AGN wind initially launched from the accretion disc. In this section we will investigate which of these processes could responsible for driving the extreme outflows observed. Following Harrison et al. (2014), we calculate the coupling efficiency which is a popular method to investigate the likely drivers of large-scale outflow. We compare the ratio of our outflow kinetic energy rate(E_{out}) with (1) the FIR AGN luminosity; (2) the FIR star formation luminosity (these two power are given by Arrigoni Battaia et al. (2018)). We also calculate the momentum-loading factor for both star-forming-driven case and AGN-driven case. Using these results we now explore the possible driving mechanisms to power this outflow.

Fig.?? shows coupling efficiency for both star-forming-driven case and AGN-driven case. We compare our result with results in Harrison et al. (2014). One way for star formation to drive large-scale outflow is by stellar winds or supernovae. An estimation of the coupling efficiency for this case is carried by Kennicutt Jr (1998), he found that the maximum coupling efficiency is $E_{out}/L_{IR,SF} \approx 0.02$, we indicate this upper limit with gray dot line in Fig.?. Based on this results, stellar winds and supernovae are unlikely to be fully responsible for the observed outflows. On the other hand, the coupling efficiency for AGN-driven case is too large which is close to 1. In the right panel of Fig.?? it shows that if the outflow is driven by AGN, it has already exceed other results with similar AGN luminosity.

Besides, if we instead consider a momentum-driven wind with momentum deposition from the radiation pressure of stars or AGN, the momentum loading factor $f_p = \log(cP_{out}/L)$ is $f_{p,SF} = 1.7$ and $f_{p,AGN} = 3.2$ respectively. nevertheless Zubovas (2018) suggests that a typical momentum loading factor for star-formation-driven case is $f_{p,SF} < 1.4$ which is lower than our estimation, this comparison also rules out the star-formation case. In the same way, we also find that $f_{p,AGN}$ is larger than the typical value.

Moreover, Shankar et al. (2006) mentions the two sources of feedback are important over different mass ranges, in particular, stellar feedback regulates the processes in low-mass galaxies while large galaxies are mainly regulated by AGN feedback. The transition mass for this two feedback mechanisms is $M_{tr} \approx 2 \times 10^{10} M_{\odot}$. By fitting the SED of source-

B, Arrigoni Battaia et al. (2018) estimates its stellar mass of source-B to be $\log(M_{star}/M_{\odot}) = 11.4^{+0.3}_{-0.2}$. Comparing with M_{tr} , this results also suggests that feedback from star formation is not the dominant reason for the outflow.

However, Zubovas (2018) also suggests there are mechanisms to reach high coupling efficiency and momentum loading factor. One possibility is hyper-Eddington SMBH growth during Compton-thick(heavily obscured) phases. In this case, SMBH would accrete material with extremely large rate and may lead to ultra fast outflows(UFO). Tombesi et al. (2013) shows that this outflow can reach the velocity $\approx 0.1c$ and will have a strong coupling with the interstellar medium(ISM). Fig.6 of Tombesi et al. (2013) shows some coupling efficiency of some UFOs ≈ 1 , but he also explains that this extremely fast and powerful outflow would occur only very close to SMBH $R \approx 1000r_s$ (where r_s is the schwarzschild radius.). He indicates that the large coupling efficiency is probably due to large environment column density $\approx 10^{24} cm^{-2}$ and highly ionized state. These two factors are consistent with the large-scale environmental conditions(MAMMOTH-1, extreme onverdensities; enomous lyman α nebula.). Nevertheless, Cai et al. (2017) suggests that the hydrogen column density is in the range $\approx 10^{20} cm^{-2}$, we indicate here that the column density in CGM maybe $10^3 cm^{-2}$ larger than this value.

In summary, based on our analyses we find the outflow is unlikely powered by star-forming processes, but we do see some similar behaviors between the outflow and UFO(high coupling efficiency and high momentum loading factor), so we conclude that this outflow maybe driven by accretion-disc winds. Although there's large uncertainty coupling efficiency estimation, this large coupling efficiency and momentum loading factor have never been seen on such a large scale. From the observation it's still unclear what kind of mechanism leads to such large coupling efficiency on such large scale(the typical coupling efficiency beyond 10kpc < 0.01), it maybe results from large column density $> 10^{24} cm^{-2}$ or very efficient cooling mechanism. Besides, it provides evidence that outflow from central quasar can truly have influence on the protocluster.

4.2. Galaxies merger

By the submillimeter observation with ALMA and data collection from literature, Arrigoni Battaia et al. (2018) fits the spectral energy distribution(SED) for Source-B, as a results he indicates that Source-B is an Ultra-Luminous Infrared Galaxy(ULIRG) with extreme far-infrared luminosity. Besides, Treister et al. (2010) shows that there is substantial observational evidence that ULIRGs(heavily obscured galaxies) are the product of the gas-rich merger of two massive galaxies. Cai et al. (2017) also shows Source-B is a strongly obscured source. On the other hand the the flux-weighted dispersion map of lyman α emission also shows velocity dispersion $> 600 km/s$ corresponding to FWHM $> 1400 km/s$ near Source-B and the large dispersion extent to projected scale $\approx 100 kpc$ (include G-5). Moreover, MAMMOTH-1 is an extreme overdensity($\delta = 10.8 \pm 2.6$), The 3 sources of

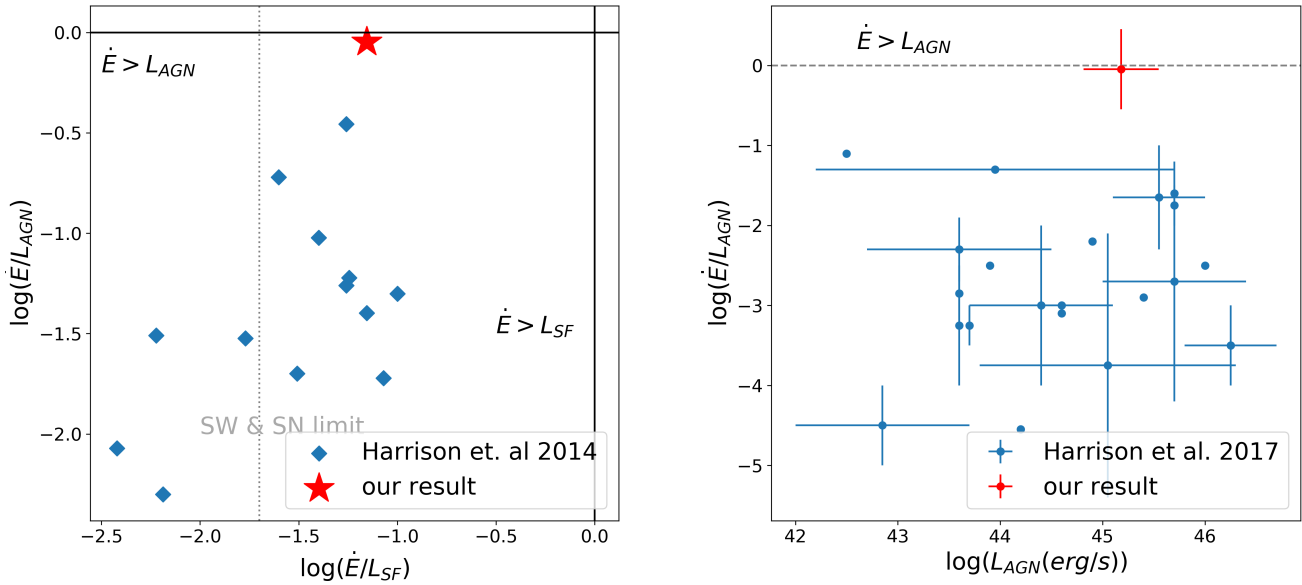


Figure 5: Left: the ratio of our estimated outflow kinetic energy rates(\dot{E}_{out}) to the AGN luminosity and to the star formation luminosity for our source(red) and sources from Harrison et al. (2014). The dashed vertical line is the estimated maximum mechanical input expected from supernovae and stellar winds. The two solid lines shows the coupling efficiency of 1. Right: Observationally determined kinetic coupling efficiencies in Harrison et al. (2018) and our result. The vertical lines show the range of values quoted or, in the case of an error bar, the quoted error on the average value. The horizontal lines show the range of bolometric luminosity for each sample. The dotted line shows coupling efficiency of 1.

source-B is within 70 kpc. All of these evidences suggests a strong galaxies merger in this region. We suggest that the physical picture of this area is like this: 3 sources of source-B is experiencing galaxy merger, center source accretes gas and material the other 2 sources, its super massive black hole(SMBH) is going through a period of rapid growth and produce strong outflow. Owing to the tidal effect between the 3 sources, lots of material is pulled out from galaxies to CGM. This can also explain why there's such large coupling efficiency between outflow and environment. Furthermore, from the velocity and dispersion map we see that the region with large dispersion extent to G-5 and there's also obvious velocity gradient on either side of G-5. This clue indicates that there may be also outflow from G-5. The large dispersion also support this point.

5. Conclusions

References

Arrigoni Battaia, F., Hennawi, J. F., Prochaska, J. X., Oñorbe, J., Farina, E. P., Cantalupo, S., & Lusso, E. 2018, Monthly Notices of the Royal Astronomical Society, 482, 3162

- Cai, Z. et al. 2017, The Astrophysical Journal, 837, 71
- Emonts, B. H., Cai, Z., Prochaska, J. X., Li, Q., & Lehnert, M. D. 2019, The Astrophysical Journal, 887, 86
- Harrison, C., Alexander, D., Mullaney, J., & Swinbank, A. 2014, Monthly Notices of the Royal Astronomical Society, 441, 3306
- Harrison, C., Costa, T., Tadhunter, C., Flütsch, A., Kakkad, D., Perna, M., & Vietri, G. 2018, Nature Astronomy, 2, 198
- Heckman, T. M., Armus, L., Miley, G. K., et al. 1990, Astrophysical Journal Supplement Series, 74, 833
- Kennicutt Jr, R. C. 1998, Annual Review of Astronomy and Astrophysics, 36, 189
- Rodrguez Zaurn, J., Tadhunter, C., Rose, M., & Holt, J. 2013, Monthly Notices of the Royal Astronomical Society, 432, 138
- Shankar, F., Lapi, A., Salucci, P., De Zotti, G., & Danese, L. 2006, The Astrophysical Journal, 643, 14
- Storey, P., & Hummer, D. 1995, Monthly Notices of the Royal Astronomical Society, 272, 41
- Tombesi, F., Cappi, M., Reeves, J., Nemmen, R., Braito, V., Gaspari, M., & Reynolds, C. 2013, Monthly Notices of the Royal Astronomical Society, 430, 1102
- Treister, E., Natarajan, P., Sanders, D. B., Urry, C. M., Schawinski, K., & Kartaltepe, J. 2010, Science, 328, 600
- Zubovas, K. 2018, Monthly Notices of the Royal Astronomical Society, 479, 3189

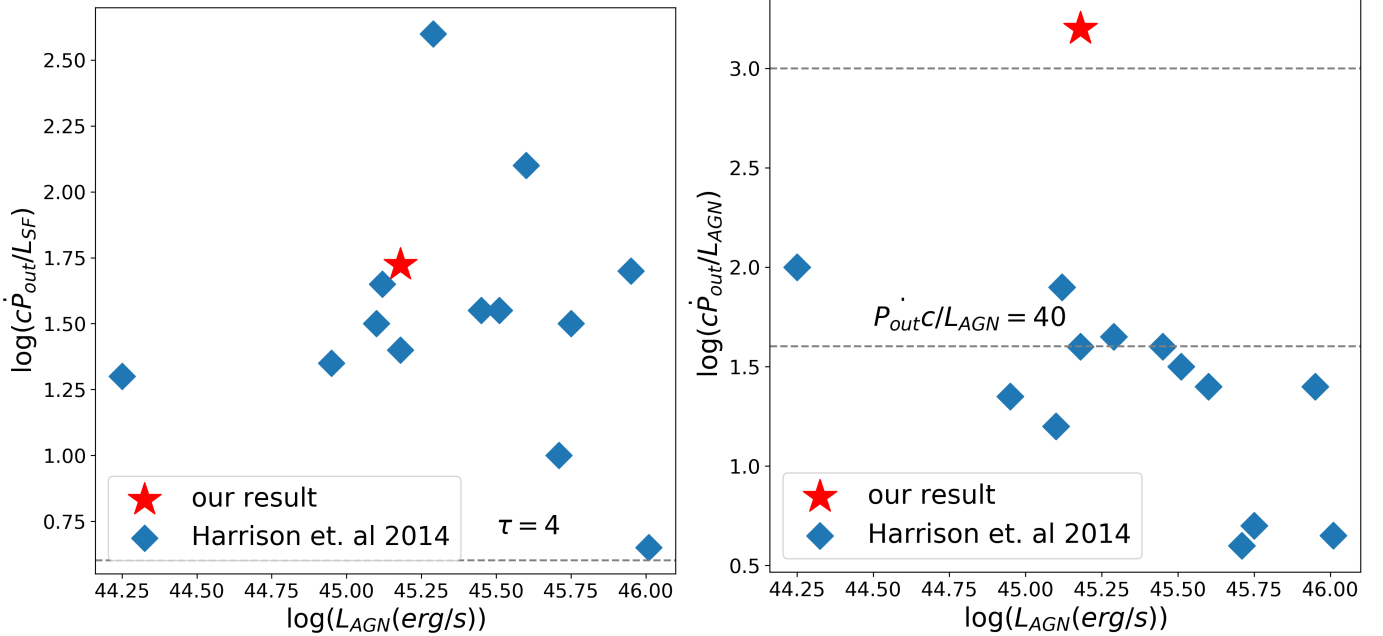


Figure 6: Left: momentum rates of the outflows(\dot{P}_{out}) normalized to the star formation luminosity L_{SF}/c versus AGN luminosity. The dashed lines represent the required optical depths if the outflows are driven by radiation pressure from star formation. Right: momentum rate of outflows normalized to AGN luminosity(L_{AGN}/c) versus AGN luminosity. Based on our assumptions, the outflows are unlikely to be purely radiatively driven, the ratio is also too high for theoretical predictions of energy-driven outflows launched by AGN accretion-disc wind.